Remote Sensing of Environment 231 (2019) 111259

Contents lists available at ScienceDirect

Remote Sensing of Environment

journal homepage: www.elsevier.com/locate/rse

Detecting hotspots of interactions between vegetation greenness and terrestrial water storage using satellite observations

Xiaoming Xie[a], Bin He[a,*], Lanlan Guo[b], Chiyuan Miao[b], Yafeng Zhang[a]

[a] State Key Laboratory of Earth Surface Processes and Resource Ecology, College of Global Change and Earth System Science, Beijing Normal University, Beijing 100875, China

[b] State Key Laboratory of Earth Surface Processes and Resource Ecology, Faculty of Geographical Science, Beijing Normal University, Beijing 100875, China

ARTICLE INFO

Edited by Jing M. Chen

Keywords:
Interaction
Terrestrial water storage
GRACE
Vegetation greenness
NDVI

ABSTRACT

Changes in water availability strongly affect vegetation growth, and vegetation can also modify land water storage by changing the land surface water balance. Here, based on the terrestrial water storage (TWS) data retrieved from the Gravity Recovery and Climate Experiment (GRACE)satellites mission and the normalized difference vegetation index (NDVI) from Jan. 2003 to Dec. 2015, we investigate the interplay between land water and vegetation greenness at a global scale. The results reveal a coherent trend with statistical significance between the terrestrial water storage anomaly (TWSA) and the NDVI in 20.90% of global vegetated lands in contrast to a non-coherent trend of 20.87% in global vegetated lands. Vegetation greenness exhibits a common 0- to 1-month delayed response to the TWSA, and significant positive TWSA-NDVI relationships appear in approximately 43.17% of global vegetated areas. A comparison study suggests that the response of vegetation greenness to the TWSA is more rapid than that to precipitation. Interactions between the TWSA and NDVI are further investigated by using the Granger causality test technique. Globally, a strong interaction between the TWSA and NDVI occurs in over 16.75% of vegetated areas. Simultaneously, vegetation greenness is found to be the Granger cause of the TWSA in over 40.34% of global vegetated areas, indicating widespread impacts of vegetation change on variations in land water storage. A case study in China suggests that vegetation greenness increase is an important reason for the decrease in the TWSA in North and Northwest China, which are traditionally water-limited-growth regions. In two humid regions, Southwest and South China, the influence of the TWSA on vegetation greenness seems to be stronger than that of vegetation greenness on the TWSA. Our study suggests that the GRACE TWS is a useful tool for investigations of interactions between vegetation greenness and land water conditions.

1. Introduction

Water is a vital prerequisite for maintaining vegetation greenness (Nemani et al., 2003). The availability of water regulates vegetation growth over approximately half of the global ecosystem (Heimann and Reichstein, 2008; Seddon et al., 2016), thereby strongly influencing the global carbon cycle (Christian et al., 2010; Humphrey et al., 2018). On the other hand, as a crucial component of terrestrial ecosystems, vegetation has great importance in regulating water balance at both regional and global scales (Donohue et al., 2009; Gerten et al., 2004; Heimann and Reichstein, 2008). Hence, a clear understanding of the interactions between land water and vegetation greenness is particularly important for forecasting future carbon cycles and water cycles (Campos et al., 2013; Heimann and Reichstein, 2008).

A large number of studies have investigated how vegetation responds to water conditions, mainly by relying on precipitation and soil water (Chen et al., 2014b; Joiner et al., 2018; Papagiannopoulou et al., 2017). For example, Wu et al. (2015) examined the response of vegetation to precipitation globally and found a prevailing time-lag effect of precipitation on vegetation greenness. By a comprehensive investigation of the response of vegetation to moisture conditions indicated by both precipitation and soil moisture, Papagiannopoulou et al. (2017) suggested that water is the leading driver of vegetation change and dominates vegetation greenness over 61% of global vegetated areas. Precipitation is the primary source of surface water and is the indicator most frequently used to explore the impact of water conditions on vegetation greenness. However, precipitation only provides indirect information about the surface water conditions (Yang et al., 2014). In comparison, soil moisture can be directly used by vegetation and is more linked with variations in plant physiological

* Corresponding author.
E-mail address: hebin@bnu.edu.cn (B. He).

https://doi.org/10.1016/j.rse.2019.111259
Received 19 September 2018; Received in revised form 6 June 2019; Accepted 7 June 2019

processes. In some water-limited-growth areas, soil moisture has been shown to be an excellent predictor of vegetation dynamics (Chen et al., 2014a; Nicolaishaw et al., 2017; Wang et al., 2018a). However, despite great improvements in soil-moisture observations and simulations, large-scale investigations of the soil moisture-vegetation relationship are still constrained by the accuracy of detecting soil moisture in the root zone (Chen et al., 2013b).

Conversely, vegetation change also strongly impacts land water conditions by directly regulating terrestrial evapotranspiration (ET) (Wei et al., 2017) and indirectly changing precipitation, runoff, and soil moisture by altering the water cycle (Zeng et al., 2018). A recent modelling study quantitatively assessed how earth greening affects the global water cycle and claimed that greening resulted in an increase of 12 ± 2.4 mm/yr in global ET and 12.1 ± 2.7 mm/yr in global precipitation over the period of 1982 to 2011, accounting for approximately 55% and 28% of the observed increase in global ET and precipitation, respectively (Zeng et al., 2018). Changes in vegetation were also found to significantly affect the land water balance in basin-scale investigations (Koirala et al., 2017; Xu et al., 2014). Koirala et al. (2017) examined the relationship between groundwater and ecosystem productivity and suggested a potential influence of ecosystem water use on groundwater table variation in some humid regions covered by forests. Wei et al.'s (2018) simulation suggested that change in vegetation cover contributed an average of 30.7% ± 22.5% to the variation in global annual runoff from 2000 to 2011. Feng et al.'s (2016) finding suggested that China's revegetation project on the Loess Plateau has greatly changed water yields across hydrological catchments due to greening-associated ET increases. The above knowledge on the impacts of vegetation growth on the land water cycle is mainly obtained through modelling, and observational evidence is still needed.

Recently, terrestrial water storage (TWS) data retrieved from the satellites of the Gravity Recovery and Climate Experiment (GRACE) have used as a new indicator to explore the hydrological impacts of vegetation greenness (Andrew et al., 2017a; Velicogna et al., 2015; Yang et al., 2014). TWS reflects all types of water stored in the continents, including canopy water, surface water, soil water, and groundwater (Tapley et al., 2004), and variations in the TWS represent integrated changes in the land water mass and have been used extensively in investigations of global and regional water storage changes and attributions, drought and flood monitoring, groundwater depletion, sea level variations, etc. (Andrew et al., 2017a; Chen et al., 2013a; Felfelani et al., 2017; Long et al., 2013; Richey et al., 2015; Scanlon et al., 2018; Thomas et al., 2014; Wang et al., 2018b). Yang et al. (2014) examined the response of vegetation greenness to the TWS anomaly (TWSA) in mainland Australia and suggested that the TWSA can capture both seasonal and interannual changes in vegetation greenness. Andrew et al. (2017b) further explored the TWSA-vegetation relationship in Australia by using the discrete wavelet transform technique, which decomposes the TWSA into different temporal frequencies. Their results show that the decomposed TWSA better explains variations in vegetation than the raw TWSA. The study of Velicogna et al. (2015) in Eurasia suggests that the TWSA not only directly impacts vegetation by changing water-availability conditions but also indirectly influences vegetation growth by regulating the response of vegetation to temperature. Although these regional investigations have suggested that vegetation growth is sensitive to the TWSA, a global examination is still required to provide a global view of the land water-vegetation relationships.

In summary, existing studies mainly focus on the one-way effect between vegetation and terrestrial water conditions, but the interactions between these two variables remain poorly understood. The present study investigates the interplay between the TWSA determined by the GRACE and vegetation greenness indicated by the normalized difference vegetation index (NDVI) at a global scale. Two main issues are addressed: (1) how vegetation responds to the hydrological conditions indicated by the TWSA and (2) the location of hot places that provide strong feedback between the TWSA and vegetation greenness.

2. Data and methodology

2.1. Data sets

The global TWS data were obtained from the GRACE JPL-Mascons product (version RL05M_1.MSCNv02CRIv02) produced by the Jet Propulsion Laboratory (JPL) of NASA using a mass concentration (mascon) approach (Watkins et al., 2015; Wiese, 2015; Wiese et al., 2016). Compared to traditional spherical harmonic solutions (Landerer and Swenson, 2012), the mascon solution has been suggested to improve the signal resolution (Save et al., 2016; Watkins et al., 2015; Wiese, 2015; Wiese et al., 2016). The JPL-Mascons product is available at a monthly temporal resolution from Apr. 2002 to Jun. 2017 and a spatial resolution of 0.5° × 0.5° latitude/longitude grid, though its native resolution is a 3° × 3° equal-area caps. Data missing for several months were simply filled in with the two-month average centred on the missing month (Andrew et al., 2017b; Long et al., 2015).

The satellite-based NDVI was used here to indicate vegetation greenness. We used the 8 km GIMMS (Global Inventory Modelling and Mapping Studies) NDVI 3 g data set retrieved from the Advanced Very High Resolution Radiometer (AVHRR) from 1982 to 2015 (Tucker et al., 2005). Despite the availability of a higher-resolution (1 km) NDVI product derived from the Moderate Resolution Imaging Spectroradiometer (MODIS), we still used the AVHRR NDVI 3 g product because it is the most commonly used product and has comparable accuracy with the MODIS NDVI in capturing vegetation change (Fensholt et al., 2012). This NDVI product is pre-treated for radiation correction, geometric correction, image enhancement, etc. (de Jong et al., 2013). The maximum value composite method was applied to reduce noise from the atmosphere, clouds, and changes in solar attitude angle and to create monthly NDVI time series (Holben, 1986).

The global monthly ET data with a spatial resolution of 0.25° used herein were obtained from the Global Land Evaporation Amsterdam Model (GLEAM) version 3.3a data set (Martens et al., 2017; Miralles et al., 2011). This product is estimated through a process-based methodology driven by gauged-based precipitation, reanalysis of air temperature and net radiation, and satellite observations of soil moisture and vegetation optical depth (Martens et al., 2017). It has a reasonable accuracy against eddy-covariance observations (Martens et al., 2017; Yang et al., 2017) and has been widely used in the study of land-atmosphere interactions (Good et al., 2017).

Global 0.5° precipitation (P) and potential evapotranspiration (PET) data sets since 1901 were obtained from the Climatic Research Unit Time Series 4.01 (CRU TS4.01). Using these two data sets, the aridity index (AI), which is defined as P/PET (Gao and Giorgi, 2008), was calculated. We divided global continents into 4 climate regions according to classifications of the AI (Findell and Eltahir, 1997): humid ($AI \geq 0.65$), sub-humid ($0.5 \leq AI < 0.65$), semi-arid ($0.2 \leq AI < 0.5$), and arid ($AI < 0.2$).

The 1° monthly vegetation water content (VWC) data from 1979 to the present were obtained from the Global Land Data Assimilation System (GLDAS) product (Rodell et al., 2004). This product contains simulations from four models: NOAH, CLM, VIC and MOS. In this study, we averaged the four simulations to obtain a VWC sequence. In addition, the 1 km MODIS global land cover product (MCD12Q1) was also used here to determine global land cover classifications.

To match the resolution of the GRACE TWS data, all data sets were processed into 0.5° × 0.5° using the nearest neighbour resampling method. In addition, our analysis was confined to the period from Jan. 2003 to Dec. 2015 because all data sets were available for this period.

2.2. Methodology

2.2.1. Calculation of TWS and NDVI anomalies

The strong seasonality of the TWS and NDVI may significantly influence investigations on the relationships between these two variables. Thus, the seasonality of these two variables was removed by calculating the monthly anomalies relative to multi-year mean values, as done by Yang et al. (2014) and Andrew et al. (2017b). Specifically, we used

$$X_{\text{anomaly}}(i,j) = X(i,j) - \frac{1}{n}\sum_{i=1}^{n} X(i,j), \tag{1}$$

where X is the monthly variable (TWS/NDVI) of interest, i is the specific month, j is the specific year, and n is the total number of years.

We noted that the seasonality of P was also removed using the above method when correlated to the NDVI.

2.2.2. Trend analysis of TWSA and NDVI

We applied the Mann–Kendall trend test to detect trends of the TWSA and NDVI over the period of Jan. 2003 to Dec. 2015. This nonparametric rank-based method was proposed by Mann (1945) and further improved by Kendall (1948, 1975), and it is frequently used for trend analysis of hydrological, meteorological, and vegetation variables (Nguyen et al., 2018). The significance of the studied trends was evaluated at a p-value < 0.05.

2.2.3. Temporal correlations between the TWSA and P

Pearson's correlation analysis was applied to explore the relationship between the NDVI and water-availability indicators (P and TWSA). In addition, some studies have shown that water availability generally leads to the behaviour of vegetation (Chen et al., 2014b; Yang et al., 2014). Therefore, the time lag of the NDVI to TWSA/P was also analysed by shifting the TWS/P time series to precede the NDVI series. A 150-month window was selected corresponding to the study period, and zero- to six-month lags were considered. The significance of the correlation coefficients was evaluated at p-value < 0.05.

2.2.4. Granger causality analysis between the TWSA and NDVI

The Granger causality test method was applied to explore the interaction between the TWSA and vegetation greenness. This test was first proposed by the economist Granger (1969) and has been widely used in many fields (Hiemstra and Jones, 1994; Papagiannopoulou et al., 2017; Sun et al., 2016). It not only explores the interrelationship between variables but also considers changes in the variable itself, thereby avoiding pseudo-correlation existing between variables. In recent years, this method has been used to explore interactions between the biosphere and atmosphere (Green et al., 2017).

Granger causality is generally defined as follows: For two time series X and Y, if the prediction effect of variable Y improves upon including the past information of variable X (as opposed to only using the past information of Y), then the variable X is considered to be the Granger cause of the variable Y (i.e., the variable X contributes to predicting the conditional distribution of the variable Y) (Sugihara et al., 2012).

The model is given as follows:

$$y_t = \sum_{i=1}^{P} (\alpha_i x_{t-i} + \beta_i y_{t-i}) + \varepsilon_1, \tag{2}$$

$$y_t = \sum_{i=1}^{P} \beta_i y_{t-i} + \varepsilon_1, \tag{3}$$

where P is the maximum lag order, N is the sample capacity, α_i and β_i are regression coefficients, and ε_1 is the error term.

An F-test was used to determine whether the estimates of Eq. (2) were statistically significantly different from the estimates of Eq. (3):

$$F = \frac{(RSS_r - RSS_m)/P}{RSS_m/(N-2P)} \propto F(P, N-2P), \tag{4}$$

The quantities RSS_m and RSS_r are the residual sum of the squares of Eqs. (3) and (4), respectively. If $F \le F_\alpha$, then the null-hypothesis does not stand, that is, X is the Granger cause of Y, where F_α is the reliability (usually set to 0.05 or 0.1).

In our study, we treated each grid as a separate problem and performed the Granger causality test between the NDVI and the TWSA grid by grid. If the prediction of the NDVI was improved by including the TWSA as a predictor, but the prediction of the TWSA was not improved by including the NDVI as a predictor, then the TWSA was said to be the unidirectional Granger cause for the NDVI. The opposite condition suggests that the NDVI was the unidirectional Granger cause of the TWSA. If the prediction of the NDVI was improved by including the TWSA as a predictor, and the prediction of the TWSA was also improved by including the NDVI as a predictor, then there was a bidirectional causality relationship between the TWSA and NDVI.

3. Results

3.1. Trends of the GRACE terrestrial water storage anomalies and vegetation greenness

Fig. 1a shows the global pattern of TWSA trends from Jan. 2003 to Dec. 2015. Over 31% of the global continents present significant decreasing trends (p-value < 0.05), with the largest drops occurring in northern Russia, southwestern and western Asia, southern South America, and northern and southern North America. In contrast, strong increases in the TWSA occur in eastern and western Russia, western Europe, eastern and central North America, southern South America, and southern Africa, all of which also accounts for 47.36% of the global continental land. This global pattern is basically consistent with that suggested by Reager et al. (2016) and is roughly consistent with some regional investigations (Ahmed et al., 2014; Asoka et al., 2017). Considering the potential impacts of the length of study periods and abnormal changes (e.g., extreme droughts and floods) on the judgement of the TWSA trends, we first tested the TWSA trends for different periods, including Jan. 2003 to Dec. 2012, Jan. 2003 to Dec. 2013, and Jan. 2003 to Dec. 2014 (Fig. S1a-c). Second, we re-examined the TWSA trends by removing the maximum and minimum anomalies for the period of Jan. 2003 to Dec. 2015 (Fig. S1d-f). We found that there is a roughly consistent pattern in the TWSA trends between these different tests. These generated patterns also agree well with the original pattern of the TWSA trends during Jan. 2003 to Dec. 2015.

Simultaneously, significant vegetation greening during the period of Jan. 2003 to Dec. 2015 occurs in eastern and southwestern Asia, western Europe, and eastern Australia, accounting for 18% of the global vegetated lands (Fig. 1b). Conversely, 36.72% of the global vegetated lands feature significant vegetation browning, mainly in western Asia, central Africa, northern South America and North America. The significant trends in the TWSA and the NDVI are coherent over a total of 20.9% of the global vegetated lands, with 12.06% of the land exhibiting significant increasing trends and 8.84% exhibiting significant decreasing trends, as shown in Fig. 1c. These coherent trends are mainly observed in relatively dry areas. Simultaneously, the non-coherent trends between the TWSA and NDVI are also found over 20.87% of the global vegetated lands.

To explore the coherence and non-coherence of those significant trends between the TWSA and the NDVI at the biomes scale, we divided the global vegetated lands into five types (forest, shrubland, savanna, grassland and agricultural land; see Table S1) according to global land cover classifications (Fig. 2). Interestingly, we found that the area ratio with coherent trends is larger than those with non-coherent trends except for forests and shrublands. The largest ratio with coherent trends is observed for grasslands, while the largest ratio with non-coherent

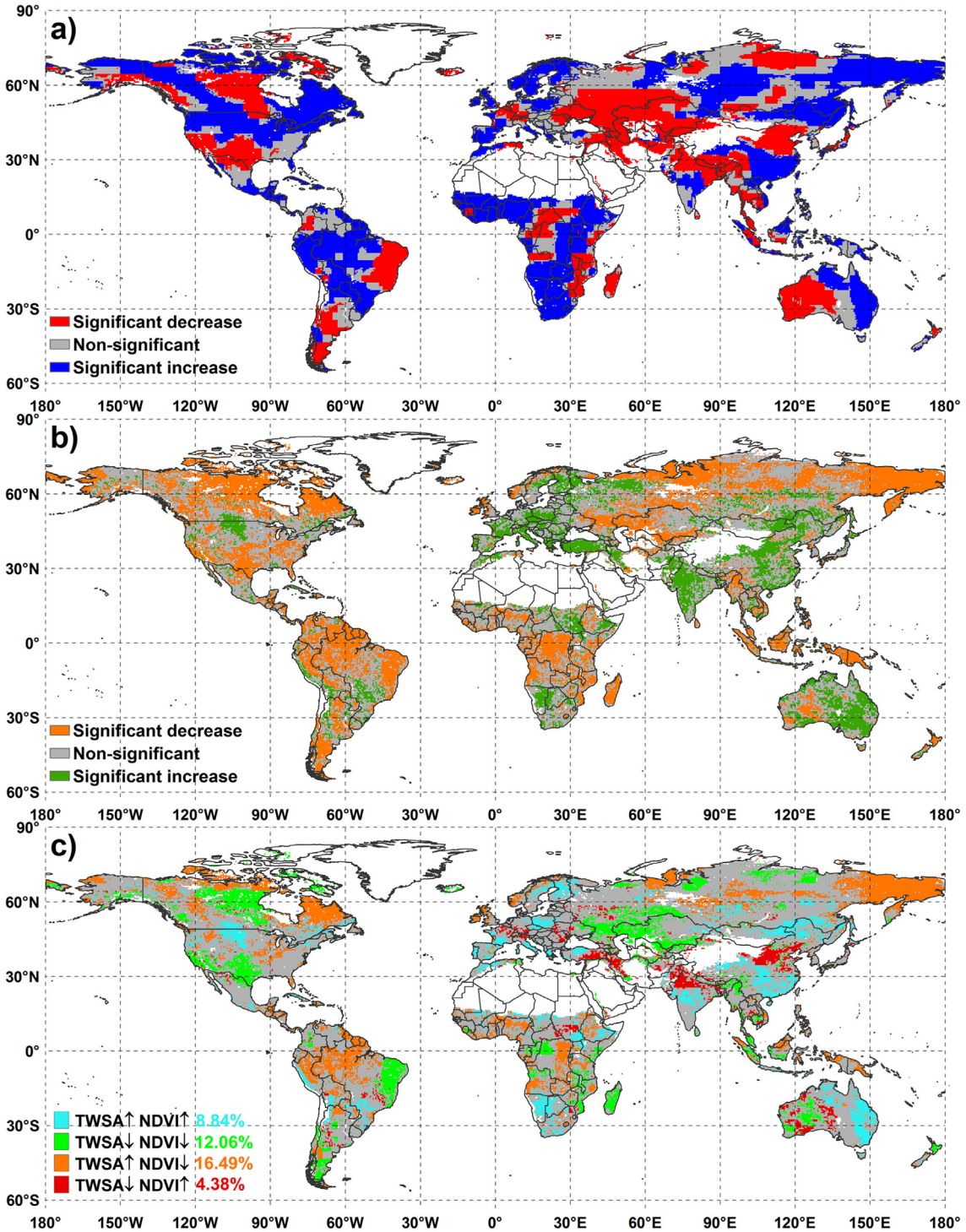

Fig. 1. Global distribution of the linear trends in a) the TWSA and b) the NDVI and c) the coherent and non-coherent trends (significant at $p < 0.05$) between the TWSA and NDVI from Jan. 2003 to Dec. 2015. Areas without significant trends are shown in grey.

trends is found for shrublands.

3.2. Response of vegetation greenness to terrestrial water storage anomalies

The response of the monthly NDVI to the TWSA was investigated using correlation analysis at the global scale without considering the lagged response of the NDVI to the TWSA (Fig. 3a). We observed an apparent decrease in the correlation coefficient associated with increasing AI (Fig. S2). Significant positive relationships are concentrated in arid, semi-arid and sub-humid regions, such as Australia, western Asia, the Indian peninsula, northern and southern Africa, southern South America, and southern North America, accounting for 30.75% of the global vegetated areas. Simultaneously, significant negative correlations mainly appear in humid regions, such as in the high northern latitudes and in areas with tropical rainforests, accounting for 16.93% of the global vegetated areas. We further investigated the NDVI-TWSA relationships using annual mean values and annual maximum and minimum values (Table S2). The largest area ratio (13.02%) with a significant positive relationship is observed between the annual maximum NDVI and TWSA, followed by that between the minimum NDVI

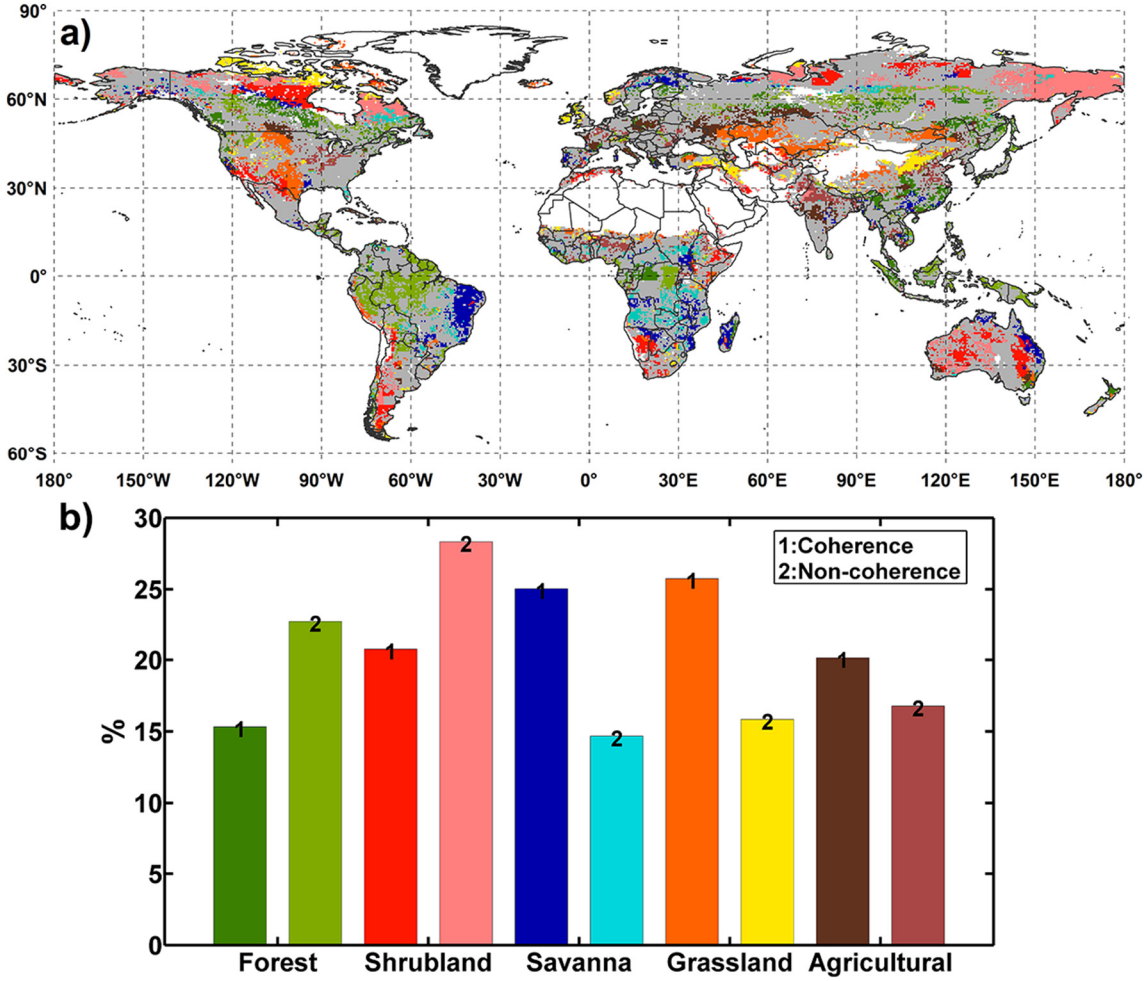

Fig. 2. a) Spatial distribution and b) area ratio of the coherent and non-coherent trends (significant at $p < 0.05$) between the TWSA and the NDVI from Jan. 2003 to Dec. 2015 for different land cover types. Areas without significant trends of TWSA/NDVI are shown in grey.

and TWSA (12.79%) and between the annual mean NDVI and TWSA (11.76%), implying an enhanced response of the NDVI under extreme water storage conditions. In addition, the NDVI-TWSA relationship was also explored at the seasonal scale (Table S3). The NDVI tends to have higher sensitivity to the TWSA in summer than in the other three seasons.

The apparent lag in the response of the NDVI to the TWSA is identified by correlating the NDVI to the TWSA with a time lag of 1 to 6 months (Fig. S3). Upon extending the length of the time lags, some weak positive relationships change to significant positive relationships. Simultaneously, the negative relationships are reduced. The maximum area ratio with significant positive relationships between these two variables occurs at 0-month lags (Fig. 5a). When we consider the lagged response, the percent of area with a significant positive correlation between the NDVI and TWSA increases from 30.75% to 43.17%. Figs. 4a and 5a demonstrate the spatial distribution of the maximum positive correlations between the NDVI and TWSA and their corresponding time lags, respectively. Spatially, short time lags (0–1) appear in arid areas covered mainly by savannas and grassland (Fig. 5d), whereas longer time lags appear in relatively humid regions covered mainly by forests, mainly concentrating in the northern middle and high latitudes.

3.3. Comparison of the NDVI response to the TWSA with that of precipitation

P is the most frequently used indicator for exploring hydrological controls of vegetation greenness. We also calculated the correlations between the NDVI and P to compare with the correlations between the NDVI and TWSA (Fig. 3b). Ignoring the potential response lag of the NDVI with respect to these hydrological indicators, the NDVI is more strongly correlated with the TWSA than with P (Fig. 3), demonstrating higher correlation coefficients and a wider extent of significant positive relationships. A total of 10.88% of the vegetated areas exhibited significant positive correlations between the NDVI and P, whereas this value was 30.75% for NDVI-TWSA. Despite differences in the values of correlation coefficients, the spatial patterns of correlations between the NDVI and the two hydrological indicators are basically coherent. Positive relationships occur in relatively dry areas, and negative relationships occur mainly in humid regions.

We also explored the response lag of the NDVI with respect to P. Figs. 4b and 5b show the maximum positive significant relationships between the NDVI and P and the corresponding time lags. Significant positive relationships between the NDVI and P are found in over 44.78% of the global vegetated areas, which are slightly higher than those between the NDVI and TWSA (43.17%). However, in terms of the maximum correlation, the NDVI variations seem to be correlated more with the TWSA than with P.

In addition, differences in the response lag of the NDVI also appear for the two indicators. In dry areas, the response lag of the NDVI to the TWSA is short or non-existent and is also shorter than that of P. In relatively humid areas, the NDVI response lag to the two indicators is relatively long. The largest proportion of significant relationships between the NDVI and TWSA is identified at 0-month lags (Fig. 5a), while

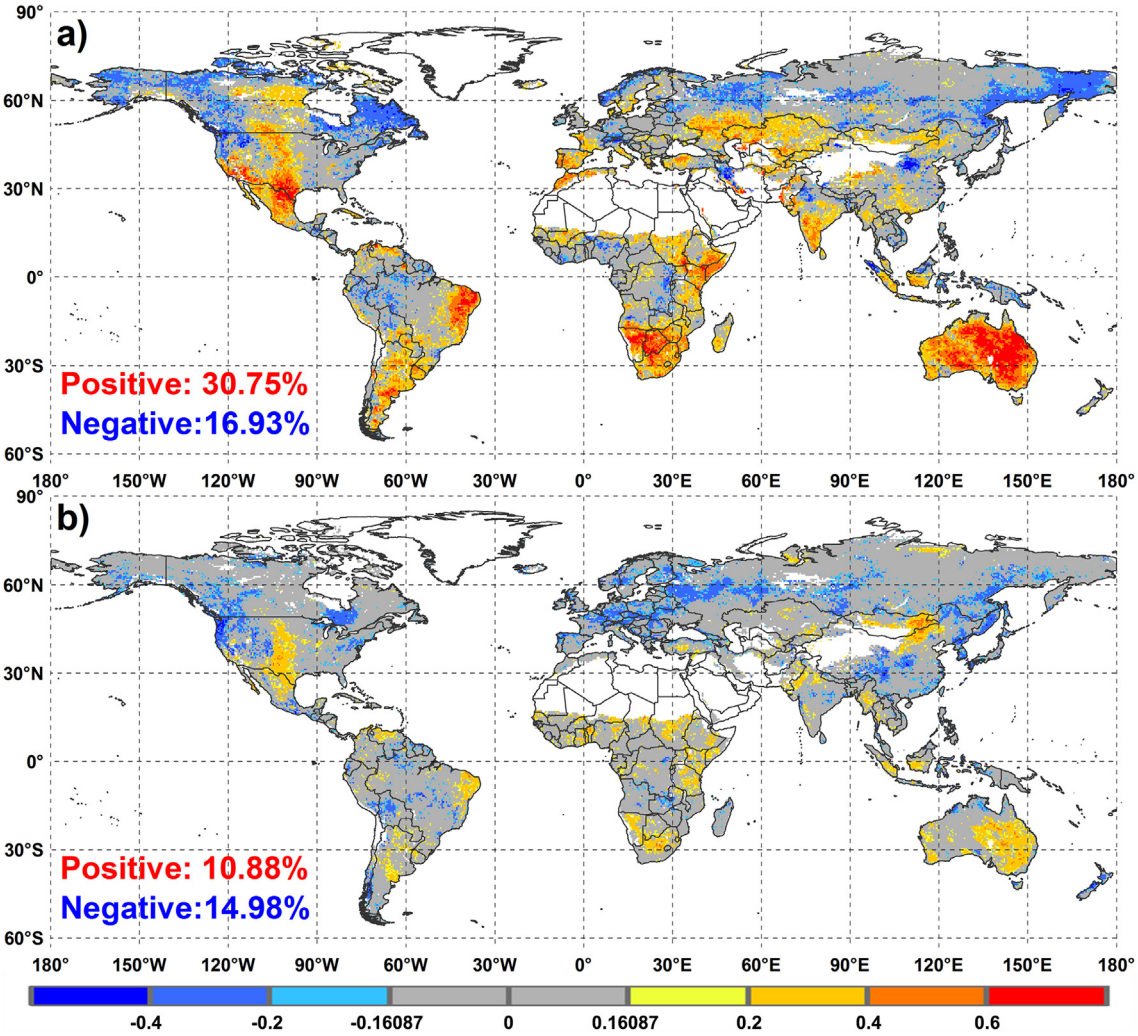

Fig. 3. Patterns of correlations of the NDVI with the a) TWSA and b) P from Jan. 2003 to Dec. 2015 without considering lags. The number in the lower left corner indicates area ratios with significant positive/negative relationships ($p < 0.05$). Areas without significant correlation are shown in grey.

that between the NDVI and P is found at 1-month lags (Fig. 5b), indicating a more rapid response of the NDVI to TWSA than to P. At the biomes scale, larger proportions of the NDVI respond to the TWSA without lags, excluding forests (Fig. 5c-d). However, a greater proportion of the NDVI tended to respond to P with a 1-month lag across all vegetation types. Overall, the TWSA demonstrates a comparable and even better performance in capturing vegetation change with P, especially in dry areas.

3.4. Causal link between terrestrial water storage anomalies and vegetation greenness

The potential interactions between the NDVI and TWSA were detected by Granger causality analysis, as shown in Fig. 6. Significant bidirectional causality relationships appear in over 16.75% of the global vegetated areas, indicating a detectable interaction between the TWSA and NDVI. These areas are scattered across continents, such as eastern Australia, southern Africa, and southwestern North America. At the biome scale, the highest proportion of interactions is observed for grasslands, followed by savannas, agricultural lands, shrublands and forests. Furthermore, the TWSA is found to be the unidirectional cause of the NDVI in over 26.21% of the vegetated areas, which are mainly distributed in drylands featured as grasslands and shrublands. The opposite conditions (i.e., that the NDVI is the unidirectional cause of the TWSA) occur both in dry and humid areas, accounting for 23.59% of the vegetated lands, which indicates that changes in vegetation may strongly affect land-water conditions. The largest area ratio with this kind of relationship is found for forests, followed by savannas, grasslands, shrublands and agricultural lands.

Overall, the TWSA is the causal cause of the NDVI in 42.96% of the vegetated areas, which are concentrated in water-limited-growth areas. In contrast, the NDVI is found to be a cause of the TWSA in 40.34% of the vegetated areas. Interestingly, we find that the areas where the NDVI is the unidirectional cause of the TWSA are mainly distributed in temperature- and radiation-limited growth areas, such as boreal forests and tropical rainforests. This suggests that vegetation dynamics in these areas will cause changes in surface hydrological processes. At the biomes scale, more extensive influences of water availability on vegetation greenness than the opposite condition are observed for all vegetation types except forests, which are featured with more extensive influences of vegetation greenness on land water conditions.

3.5. A case study in China

To better understand the interaction between the TWSA and NDVI, a case study was carried out in China, which has a vast territory with various climate zones and vegetation types. The whole study region was further divided into 9 sub-regions according to Peng et al.'s (2011) study for convenience of analysis (Fig. 7a), and the TWSA–NDVI relationship was explored for each region using Pearson's correlation

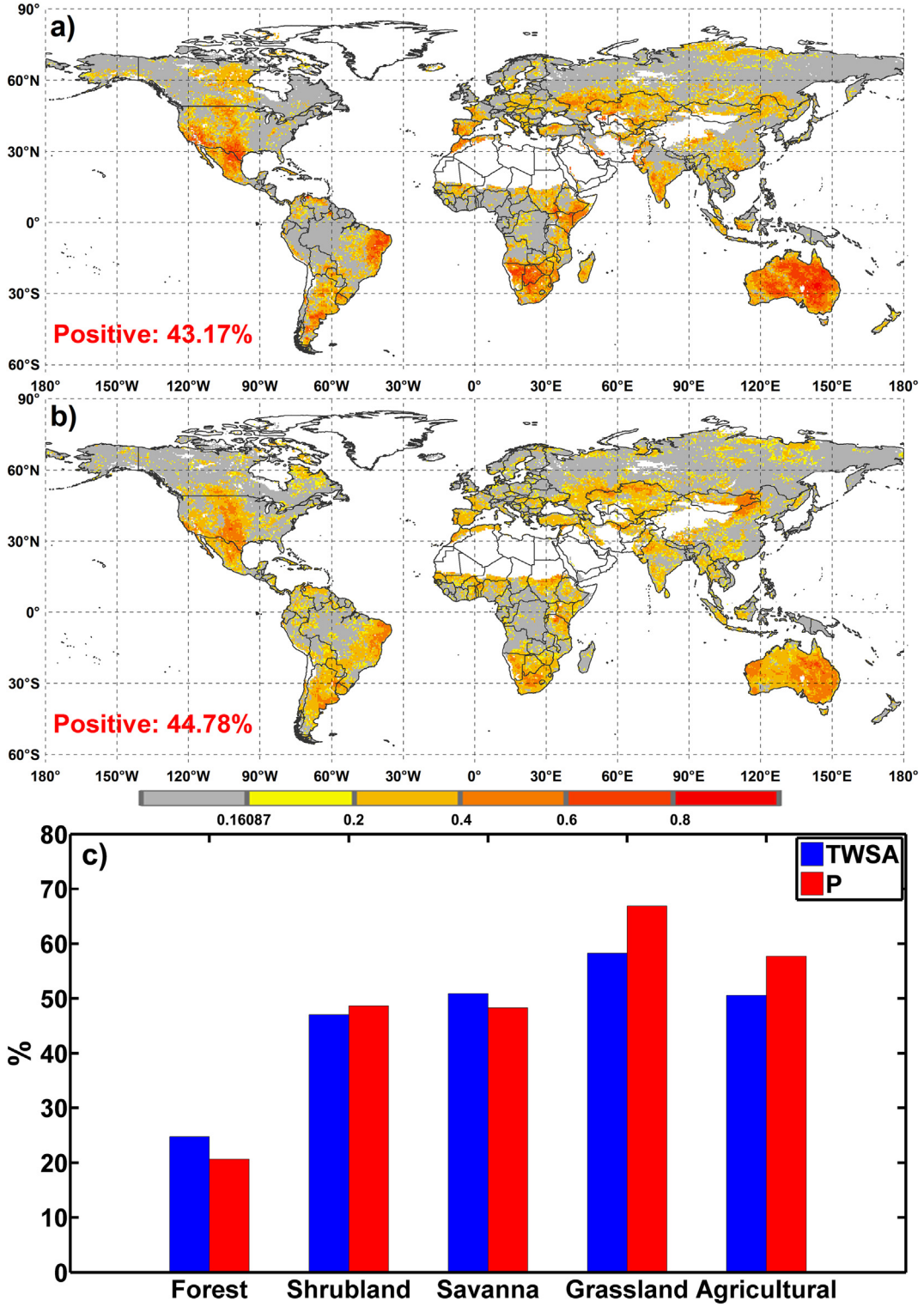

Fig. 4. Maximum correlation coefficients of the NDVI with the a) TWSA and b) P (only significant relationships are shown) and corresponding c) area ratios for each land cover classification. Areas without significant correlations are shown in grey.

analysis and the Granger causality test. Fig. 7b shows the maximum correlation between the regional mean TWSA and the NDVI when time lag was considered. A significant negative relationship is observed in the Northwest region (NW) and the North region (NO), while a significant positive relationship occurs in the Inner Mongolia region (IM), the Northeast region (NE), the Central region (CE), the Southwest region (SW) and the South region (SO). In the East region (EA) and the Qinghai-Tibet region (QT), the TWSA and NDVI present a weak negative correlation. Strong interactions determined by the Granger causality test between the TWSA and NDVI are observed in over 16.63% of the vegetated areas in China (Fig. S4e) and are mainly distributed in the SO and NO. The NDVI is identified as the unidirectional cause of the TWSA in over 24.11% of the vegetated areas located in the NW, IM, EA, and NE. On the other hand, the TWSA is found to be the unidirectional

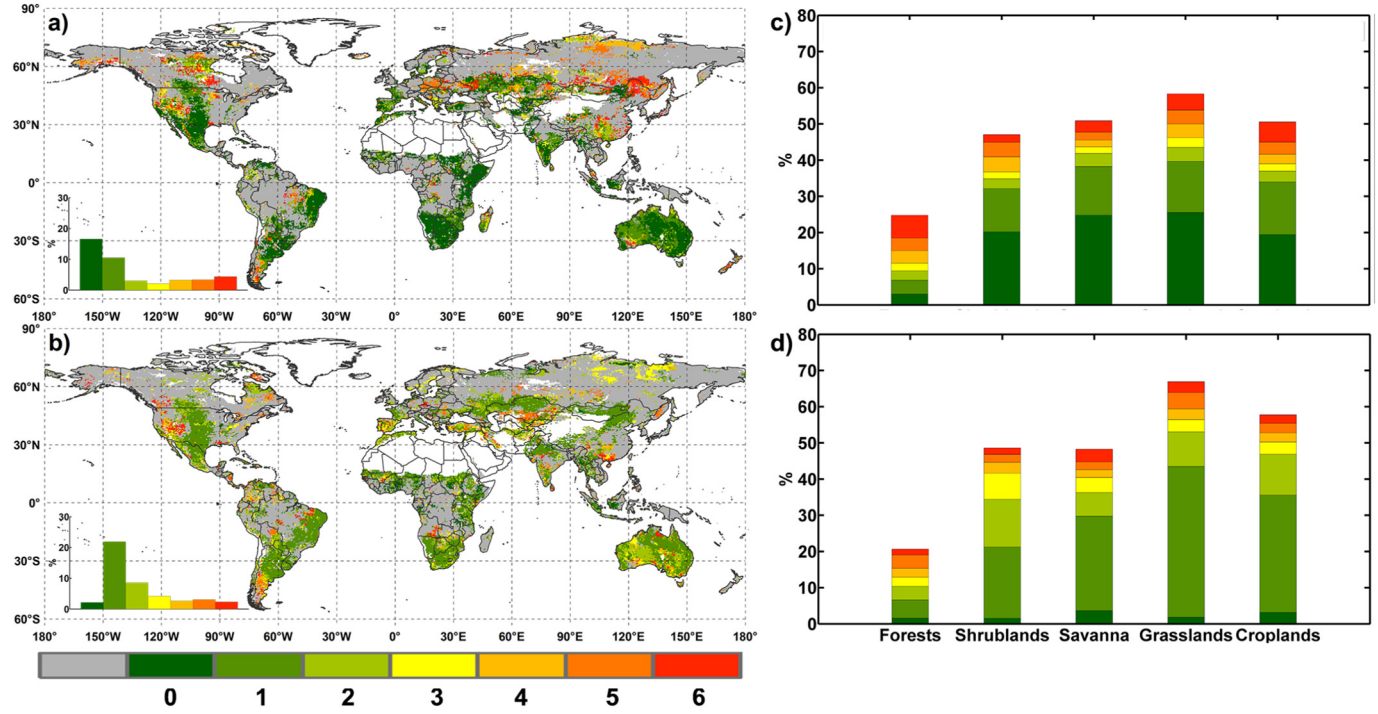

Fig. 5. The time lags of the NDVI to a) TWSA and b) P corresponding to the maximum coefficient, as shown in Fig. 4. c) and d) indicate area ratios with land cover types. Areas without significant correlations are shown in grey.

cause of the NDVI in over 26.13% of the vegetated areas, which are concentrated in the SW and CE.

Combining the results from the correlation analysis and the Granger causality test, we found that in two traditional water-limited-growth regions, the NW and NO, extensive influences of vegetation greenness on the TWSA are observed (Fig. 8a and b). In contrast, in two traditional radiation-limited-growth regions, SW and SO, we found widespread influences of the TWSA on vegetation greenness (Fig. 8c and d). To explore the potential reasons, we further examined the interannual variation in the TWSA, NDVI and ET in these four regions. ET was included here, as it is a main way by which vegetation changes the TWSA. The TWSAs in the NW and NO regions both show a decreasing trend (Fig. 8a, Fig. S4a), while the NDVI and ET present an increasing trend (Fig. 8a, Fig. S4b and S4c). According to previous studies (Deng and Chen, 2017; Xie et al., 2018), warming-caused snowmelt and enhanced ET might be responsible for the TWSA decrease west of the NW region. The eastern part of the NW is the Loess Plateau, where a revegetation programme was launched in 1999. The revegetation programme has been suggested to increase vegetation growth and associated ET (Feng et al., 2016; Jin et al., 2017; Pei et al., 2017). The promoted ET is also found to decrease surface water yield and exert pressure on land water availability (Feng et al., 2016; Jin et al., 2017). This can partly explain the decreasing TWSA. The NO is a typical irrigated agricultural region, and groundwater extraction for irrigation caused a rapid decrease in the

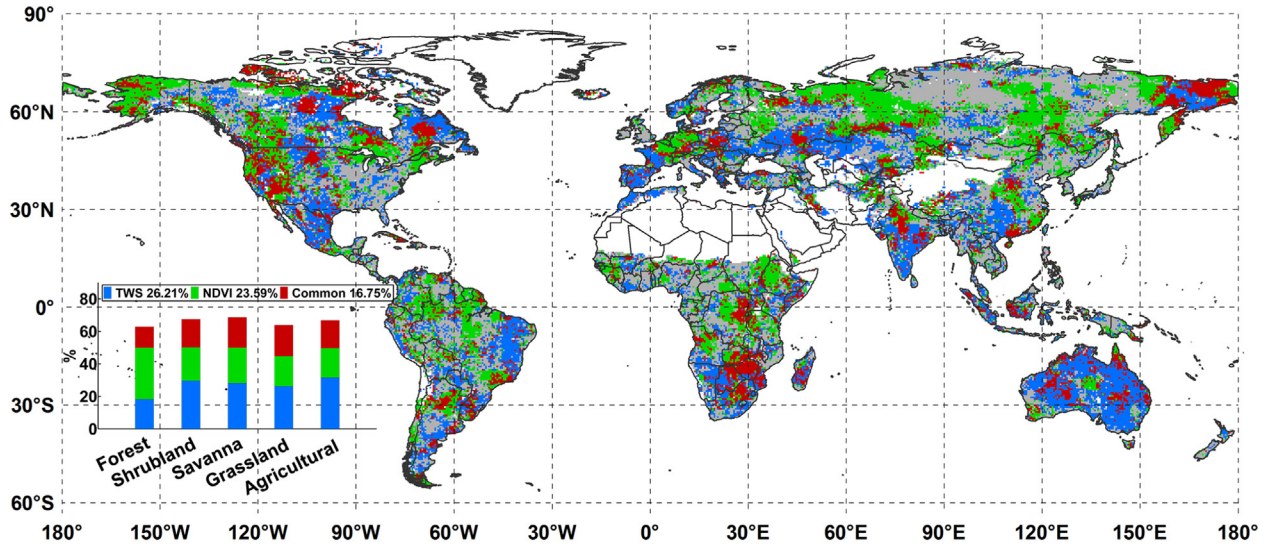

Fig. 6. Granger causality between the NDVI and TWSA. The red areas are identified with bidirectional causality relationships between the water conditions and the NDVI; the green indicates that the NDVI is the unidirectional cause of the water conditions; the blue indicates that the water conditions are the unidirectional cause of the NDVI. Areas without significant causal links are shown in grey. (For interpretation of the references to colour in this figure legend, the reader is referred to the web version of this article.)

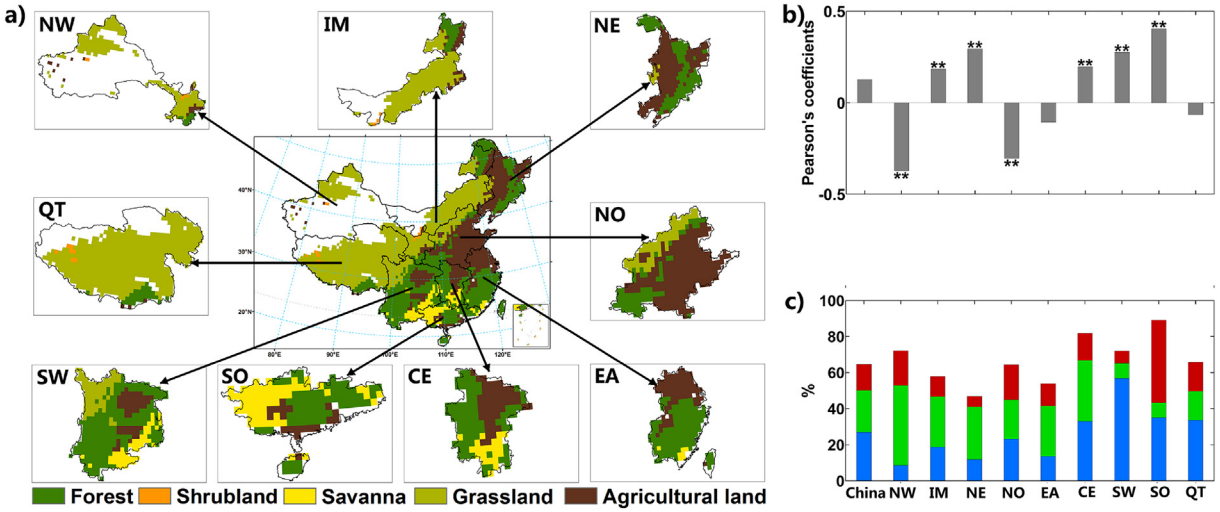

Fig. 7. a) Spatial distributions of land cover types and 9 sub-regions, b) correlations and c) Granger causal links between the TWSA and NDVI in 9 regions during Jan. 2003 to Dec. 2015. The 9 regions are the Northwest (NW), Inner Mongolia (IM), Northeast (NE), North (NO), East (EA), Central (CE), Southwest (SW), and South (SO) China and the Qinghai-Tibet (QT) region of China.

TWSA. Pan et al. (2017) determined the groundwater irrigation-induced ET using the GRACE TWS in the Haihe River basin in the NO and suggested that it contributes to a 12% increase in total ET. In summary, greening-associated ET increases play an important role in TWSA variation in the NW and NO regions.

In both the SW and SO regions, the TWSA demonstrates a significant increasing trend accompanied by an increase in the NDVI (Fig. 8c and d, Fig. S4a and S4b). We also observed significant positive relationships between the TWSA and NDVI in these two regions (Fig. S4d). However, according to previous investigations (Hou et al., 2015; Peng et al., 2011), vegetation greenness in these two regions usually negatively responds to precipitation, implying that water availability condition is not a driver of vegetation change. The potential reason may be that these studies ignored the lag of the NDVI to precipitation, which is clearly illustrated by the difference between Figs. 3b and 4b. Despite the increase in the TWSA and the NDVI, ET in both regions exhibits a weak decreasing trend, implying that ET is not a main reason for the TWSA change. The above analysis may explain why more extensive influences of the TWSA on vegetation greenness than under the opposite conditions are observed in these two regions.

4. Discussion and conclusions

The TWS derived from the GRACE provides an integrated measurement of land water availability. Using TWS as a tool, this study investigates the hydrological controls of vegetation greenness and examines the interactions between land water and vegetation greenness. Although various studies have explored how the TWSA affects vegetation greenness at the regional scale (Andrew et al., 2017b; Yang et al., 2014), there is no systematic modelling that actually links the NDVI with the TWSA, particularly at a global scale. Vegetation greenness responds positively to the TWSA in traditional water-limited-growth areas but responds negatively in radiation- or temperature-limited-growth areas. This pattern agrees roughly with previous investigations

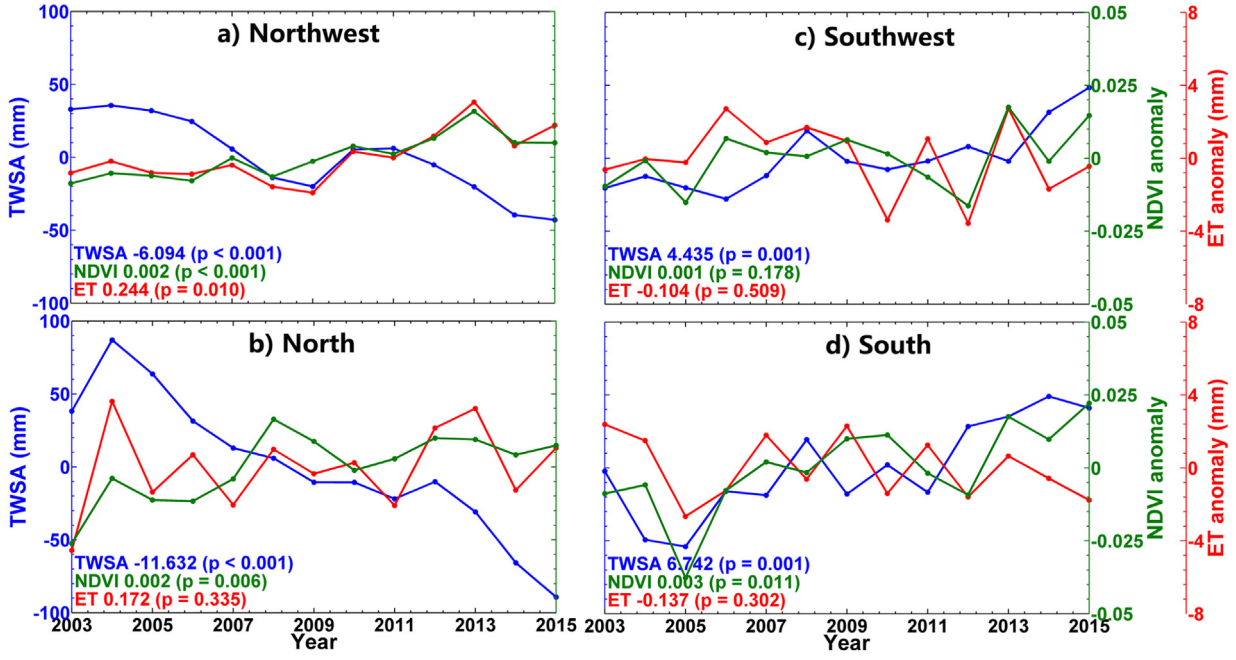

Fig. 8. Interannual variations in the TWSA, NDVI, and ET from 2003 to 2015 in a) Northwest, b) North, c) Southwest and d) South China.

based on P and SM (Papagiannopoulou et al., 2017; Vicente-Serrano et al., 2013). The significantly positive NDVI-TWSA relationship accounts for 43.17% of the global vegetated areas. This ratio is comparable with a previous study that examined the response of global ecosystem productivity to hydrological conditions based on the aridity index (Nemani et al., 2003). In addition, as previously reported (Andrew et al., 2017b), the response of vegetation greenness lags behind the TWSA, and the length of the time lags seems to depend on the climate aridity, with more arid climates corresponding to shorter time lags. The GRACE TWS reflects all kinds of water stored in land, among which the vegetation water content (VWC) is an important component. To examine whether the observed positive relationships between the NDVI and TWSA are caused by the intrinsic relationship between the NDVI and VWC, we tested the response of the NDVI to VWC obtained from GLDAS, as shown in Fig. S5. Significant positive relationships are observed in over 9.11% of the vegetated areas scattered throughout the dry regions, suggesting the potential influence of the VWC on the NDVI-TWSA relationships determined in this study.

Previous studies have suggested that in Australia, the GRACE is a better indicator than soil moisture or precipitation for understanding hydrological influences on vegetation (Andrew et al., 2017b; Yang et al., 2014). The present comparison study suggests that globally, vegetation greenness tends to be more sensitive to the TWSA than to P. This result may be explained by the fact that the TWSA provides a better representation of the actual water availability condition for plants (Yang et al., 2014), whereas precipitation only provides indirect information about surface water conditions (Chen et al., 2013a). Rainforests are traditionally considered to be not water-limited growth areas. However, we found that the NDVI sensitively responds to the TWSA in some areas of the Congo rainforest (Fig. 4a). This could be supported by Zhou et al.'s (2014) study. They found that a rainfall decrease caused a decline in vegetation greenness from 2000 to 2012. As mentioned in the introduction, TWS reflects all types of water stored in land, so anomalies in the TWS can result from any component of land water (e.g., surface water, soil water, and groundwater) (Felfelani et al., 2017; Soni and Syed, 2015). In other words, the TWSA does not necessarily reflect the change in water available conditions for vegetation greenness. For example, deficits in groundwater may have no influence on short-root plants. Generally, compared to P, the TWSA provides more direct information on the availability of water for plants and better explain changes in vegetation. This may be confirmed by the finding that vegetation responds to the TWSA more promptly than to P.

In addition to the control exerted by land water over vegetation greenness, plants can also regulate land water conditions (Liu et al., 2016). This study provides a preliminary analysis of the interactions between the TWSA and NDVI by using the Granger causality test. Strong interactions occur in over 16.75% of the global vegetated areas. In addition, the TWSA is identified as the Granger cause of the NDVI in over 42.96% of global vegetated areas, which are concentrated in traditional water-limited growth areas. This is roughly consistent with the findings from the correlation test between the TWSA and NDVI in both the total area ratio and spatial patterns. Conversely, vegetation greenness is also found to strongly influence land water conditions over the continents (Koirala et al., 2017). In this study, the NDVI is detected as the Granger cause of the TWSA in over 40.34% of the global vegetated areas, indicating an extensive influence of vegetation change on land water storage. In some humid ecosystems (e.g., at middle and high latitudes), vegetation is the Granger cause of the TWSA, but the TWSA is not the Granger cause of vegetation. A possible explanation is that the vegetation in these regions is not limited by water but by temperature or solar radiation (Nemani et al., 2003; Seddon et al., 2016). However, these regions are mainly covered by forests with high ET rates. Therefore, ET change caused by the variation in vegetation greenness will inevitably influence the land water conditions (Wei et al., 2017). A recent study also revealed the great impact of ecosystem water use on groundwater level change in humid forests (Koirala et al., 2017).

The results from this study are mainly based on satellite products. Hence, they will be inevitably subject to uncertainties associated with satellite retrievals. For example, the satellite NDVI has been found to frequently suffer from saturation problems in high vegetation cover areas (e.g., tropic forests) (Huete et al., 1997; Morton et al., 2014; Nicholson and Farrar, 1994). In addition, its accuracy is easily influenced by the contamination of atmospheric conditions (e.g., clouds and aerosols), shifts or degradation of sensors, etc. (Pinzon and Tucker, 2014; Tian et al., 2015). Uncertainties associated with the GRACE TWS should not be ignored. Although the mascon solution has been suggested to greatly reduce the signal loss (Watkins et al., 2015; Wiese et al., 2016), caution is still needed when it is used near coastal regions (Wiese et al., 2016). Additionally, as described in Section 2.1, the original resolution of the GRACE TWS is $3^\circ \times 3^\circ$ (Watkins et al., 2015), which indicates that the TWSA signal of the downscaled $0.5^\circ \times 0.5^\circ$ grid used for analysis is independent of its surrounding grids. Therefore, the different relationships between the TWSA and NDVI built in this study should not be fully interpreted as the differences in vegetation type because each $3^\circ \times 3^\circ$ grid may comprise several vegetation types. It should also be noted that the detection of Granger causality between the NDVI and TWSA does not imply a direct physical mechanism existing between these two variables. Therefore, our study only indicates possible causality links by a statistical method.

Overall, the results confirm the basic feasibility of using the GRACE TWS as a tool to explore the hydrological impact of plant greenness and the interaction between vegetation greenness and land water conditions. In particular, the TWS is found to be an ideal indicator to investigate the influence of vegetation change on land water conditions. The interaction established herein between the TWSA and vegetation can help to improve the understanding of the global terrestrial water and carbon cycle. However, this study only provides a preliminary investigation of TWSA-vegetation relationships; more in-depth studies focused on some specific areas, such as Andrew et al. (2017b) in Australia, are still needed.

Acknowledgements

This work was supported by the Strategic Priority Research Program of the Chinese Academy of Sciences (grant no. XDA20060402) and the National Key Scientific Research and Development Program of China (grant no. 2017YFA0603601). We thank the three reviewers for their very insightful comments on this paper.

Appendix A. Supplementary data

Supplementary data to this article can be found online at https://doi.org/10.1016/j.rse.2019.111259.

References

Ahmed, M., Sultan, M., Wahr, J., Yan, E., 2014. The use of GRACE data to monitor natural and anthropogenic induced variations in water availability across Africa. Earth Sci. Rev. 136, 289–300.

Andrew, R., Guan, H., Batelaan, O., 2017a. Estimation of GRACE water storage components by temporal decomposition. J. Hydrol. 552, 341–350.

Andrew, R.L., Guan, H., Batelaan, O., 2017b. Large-scale vegetation responses to terrestrial moisture storage changes. Hydrol. Earth Syst. Sci. 21, 4469–4478.

Asoka, A., Gleeson, T., Wada, Y., Mishra, V., 2017. Relative contribution of monsoon precipitation and pumping to changes in groundwater storage in India. Nat. Geosci. 10, 109–117.

Campos, G.E.P., Moran, M.S., Huete, A., Zhang, Y.G., Bresloff, C., Huxman, T.E., Eamus, D., Bosch, D.D., Buda, A.R., Gunter, S.A., Scalley, T.H., Kitchen, S.G., McClaran, M.P., McNab, W.H., Montoya, D.S., Morgan, J.A., Peters, D.P.C., Sadler, E.J., Seyfried, M.S., Starks, P.J., 2013. Ecosystem resilience despite large-scale altered hydroclimatic conditions. Nature 494, 349–352.

Chen, Y., Velicogna, I., Famiglietti, J.S., Randerson, J.T., 2013a. Satellite observations of terrestrial water storage provide early warning information about drought and fire season severity in the Amazon. J. Geophys. Res. Biogeosci. 118, 495–504.

Chen, Y.Y., Yang, K., Qin, J., Zhao, L., Tang, W.J., Han, M.L., 2013b. Evaluation of AMSR-E retrievals and GLDAS simulations against observations of a soil moisture network

on the central Tibetan Plateau. J. Geophys. Res.-Atmos. 118, 4466–4475.
Chen, B.Z., Xu, G., Coops, N.C., Ciais, P., Innes, J.L., Wang, G.Y., Myneni, R.B., Wang, T.L., Krzyzanowski, J., Li, Q.L., Cao, L., Liu, Y., 2014a. Changes in vegetation photosynthetic activity trends across the Asia-Pacific region over the last three decades. Remote Sens. Environ. 144, 28–41.
Chen, T., de Jeu, R.A.M., Liu, Y.Y., van der Werf, G.R., Dolman, A.J., 2014b. Using satellite based soil moisture to quantify the water driven variability in NDVI: A case study over mainland Australia. Remote Sens. Environ. 140, 330–338.
Christian, B., Markus, R., Enrico, T., Philippe, C., Martin, J., Nuno, C., Christian, R.D., M Altaf, A., Dennis, B., Bonan, G.B., 2010. Terrestrial gross carbon dioxide uptake: global distribution and covariation with climate. Science 329, 834–838.
Deng, H., Chen, Y., 2017. Influences of recent climate change and human activities on water storage variations in Central Asia. J. Hydrol. 544, 46–57.
Donohue, R.J., McVicar, T.R., Roderick, M.L., 2009. Climate-related trends in Australian vegetation cover as inferred from satellite observations, 1981-2006. Glob. Chang. Biol. 15, 1025–1039.
Felfelani, F., Wada, Y., Longuevergne, L., Pokhrel, Y.N., 2017. Natural and human-induced terrestrial water storage change: a global analysis using hydrological models and GRACE. J. Hydrol. 553, 105–118.
Feng, X., Fu, B., Piao, S., Wang, S., Ciais, P., Zeng, Z., Lü, Y., Zeng, Y., Li, Y., Jiang, X., 2016. Revegetation in China's loess plateau is approaching sustainable water resource limits. Nat. Clim. Chang. 6, 1019.
Fensholt, Rasmus, PROUD, Simon, R., 2012. Evaluation of earth observation based global long term vegetation trends — comparing GIMMS and MODIS global NDVI time series. Remote Sens. Environ. 119, 131–147.
Findell, K.L., Eltahir, E.A., 1997. An analysis of the soil moisture-rainfall feedback, based on direct observations from Illinois. Water Resour. Res. 33, 725–735.
Gao, X., Giorgi, F., 2008. Increased aridity in the Mediterranean region under greenhouse gas forcing estimated from high resolution simulations with a regional climate model. Glob. Planet. Chang. 62, 195–209.
Gerten, D., Schaphoff, S., Haberlandt, U., Lucht, W., Sitch, S., 2004. Terrestrial vegetation and water balance—hydrological evaluation of a dynamic global vegetation model. J. Hydrol. 286, 249–270.
Good, S.P., Moore, G.W., Miralles, D.G., 2017. A Mesic maximum in biological water use demarcates biome sensitivity to aridity shifts. Nat. Ecol. Evol. 1, 1883–1888.
Granger, C.W., 1969. Investigating causal relations by econometric models and cross-spectral methods. Econometrica 424–438.
Green, J.K., Konings, A.G., Alemohammad, S.H., Berry, J., Entekhabi, D., Kolassa, J., Lee, J.-E., Gentine, P., 2017. Regionally strong feedbacks between the atmosphere and terrestrial biosphere. Nat. Geosci. 10, 410–414.
Heimann, M., Reichstein, M., 2008. Terrestrial ecosystem carbon dynamics and climate feedbacks. Nature 451, 289–292.
Hiemstra, C., Jones, J.D., 1994. Testing for linear and nonlinear granger causality in the stock price- volume relation. J. Financ. 49, 1639–1664.
Holben, B.N., 1986. Characteristics of maximum-value composite images from temporal Avhrr data. Int. J. Remote Sens. 7, 1417–1434.
Hou, W., Gao, J., Wu, S., Dai, E., 2015. Interannual variations in growing-season NDVI and its correlation with climate variables in the southwestern karst region of China. Remote Sens. 7, 11105–11124.
Huete, A.R., Liu, H.Q., Leeuwen, W.J.D.V., 1997. Use of vegetation indices in forested regions: issues of linearity and saturation. In: Geoscience & Remote Sensing, Igarss 97 Remote Sensing-a Scientific Vision for Sustainable Development. IEEE International, pp. 1966–1968.
Humphrey, V., Zscheischler, J., Ciais, P., Gudmundsson, L., Sitch, S., Seneviratne, S.I., 2018. Sensitivity of atmospheric CO2 growth rate to observed changes in terrestrial water storage. Nature 560, 628–631.
Jin, Z., Liang, W., Yang, Y., Zhang, W., Yan, J., Chen, X., Li, S., Mo, X., 2017. Separating vegetation greening and climate change controls on evapotranspiration trend over the Loess Plateau. Sci. Rep. 7, 8191.
Joiner, J., Yoshida, Y., Anderson, M., Holmes, T., Hain, C., 2018. Global relationships among traditional reflectance vegetation indices (NDVI and NDII), evapotranspiration (ET), and soil moisture variability on weekly timescales. Remote Sens. Environ. 219, 339–352.
de Jong, R., Verbesselt, J., Zeileis, A., Schaepman, M.E., 2013. Shifts in global vegetation activity trends. Remote Sens. 5, 1117–1133.
Kendall, M.G., 1948. Rank Correlation Methods.
Kendall, M., 1975. Multivariate Analysis. Charles Griffin & Company Ltd.
Koirala, S., Jung, M., Reichstein, M., Graaf, I.E.M.D., Camps-Valls, G., Ichii, K., Papale, D., Ráduly, B., Schwalm, C.R., Tramontana, G., 2017. Global distribution of groundwater-vegetation spatial covariation: global groundwater-vegetation relations. Geophys. Res. Lett. 44, 4134–4142.
Landerer, F.W., Swenson, S.C., 2012. Accuracy of scaled GRACE terrestrial water storage estimates. Water Resour. Res. 48 (W04531.04531-W04531.04511).
Liu, Y., Xiao, J., Ju, W., Xu, K., Zhou, Y., Zhao, Y., 2016. Recent trends in vegetation greenness in China significantly altered annual evapotranspiration and water yield. Environ. Res. Lett. 11, 094010.
Long, D., Scanlon, B.R., Longuevergne, L., Sun, A.Y., Fernando, D.N., Save, H., 2013. GRACE satellite monitoring of large depletion in water storage in response to the 2011 drought in Texas. Geophys. Res. Lett. 40, 3395–3401.
Long, D., Yang, Y.T., Wada, Y., Hong, Y., Liang, W., Chen, Y.N., Yong, B., Hou, A.Z., Wei, J.F., Chen, L., 2015. Deriving scaling factors using a global hydrological model to restore GRACE total water storage changes for China's Yangtze River Basin. Remote Sens. Environ. 168, 177–193.
Mann, H.B., 1945. Nonparametric tests against trend. Econometrica 245–259.
Martens, B., Miralles, D.G., Lievens, H., van der Schalie, R., de Jeu, R.A.M., Fernandez-Prieto, D., Beck, H.E., Dorigo, W.A., Verhoest, N.E.C., 2017. GLEAM v3: satellite-based land evaporation and root-zone soil moisture. Geosci. Model Dev. 10, 1903–1925.
Miralles, D.G., Holmes, T.R.H., De Jeu, R.A.M., Gash, J.H., Meesters, A.G.C.A., Dolman, A.J., 2011. Global land-surface evaporation estimated from satellite-based observations. Hydrol. Earth Syst. Sci. 15, 453–469.
Morton, D.C., Jyoteshwar, N., Carabajal, C.C., Jacqueline, R., Michael, P., Cook, B.D., Vermote, E.F., Harding, D.J., North, P.R.J., 2014. Amazon forests maintain consistent canopy structure and greenness during the dry season. Nature 506, 121–221.
Nemani, R.R., Keeling, C.D., Hashimoto, H., Jolly, W.M., Piper, S.C., Tucker, C.J., Myneni, R.B., Running, S.W., 2003. Climate-driven increases in global terrestrial net primary production from 1982 to 1999. Science 300, 1560–1563.
Nguyen, P., Thorstensen, A., Sorooshian, S., Hsu, K., Aghakouchak, A., Ashouri, H., Tran, H., Braithwaite, D., 2018. Global precipitation trends across spatial scales using satellite observations. Bull. Am. Meteorol. Soc. 99, 689–697.
Nicholson, S.E., Farrar, T.J., 1994. The influence of soil type on the relationships between NDVI, rainfall, and soil moisture in semiarid Botswana. I. NDVI response to rainfall. Remote Sens. Environ. 50, 107–120.
Nicolaishaw, N., Zscheischler, J., Hirschi, M., Gudmundsson, L., Seneviratne, S.I., 2017. A drought event composite analysis using satellite remote-sensing based soil moisture. Remote Sens. Environ. 203, 216–225.
Pan, Y., Zhang, C., Gong, H., Yeh, P.J.F., Shen, Y., Guo, Y., Huang, Z., Li, X., 2017. Detection of human-induced evapotranspiration using GRACE satellite observations in the Haihe River basin of China. Geophys. Res. Lett. 44, 190–199.
Papagiannopoulou, C., Miralles, D.G., Dorigo, W.A., Verhoest, N.E.C., Depoorter, M., Waegeman, W., 2017. Vegetation anomalies caused by antecedent precipitation in most of the world. Environ. Res. Lett. 12, 074016.
Pei, T., Wu, X., Li, X., Zhang, Y., Shi, F., Ma, Y., Wang, P., Zhang, C., 2017. Seasonal divergence in the sensitivity of evapotranspiration to climate and vegetation growth in the Yellow River Basin, China. J. Geophys. Res. Biogeosci. 122, 103–118.
Peng, S., Chen, A., Xu, L., Cao, C., Fang, J., Myneni, R.B., Pinzon, J.E., Tucker, C.J., Piao, S., 2011. Recent change of vegetation growth trend in China. Environ. Res. Lett. 6, 044027.
Pinzon, J.E., Tucker, C.J., 2014. A non-stationary 1981–2012 AVHRR NDVI 3g time series. Remote Sens. 6, 6929–6960.
Reager, J., Gardner, A., Famiglietti, J., Wiese, D., Eicker, A., Lo, M.-H., 2016. A decade of sea level rise slowed by climate-driven hydrology. Science 351, 699–703.
Richey, A.S., Thomas, B.F., Lo, M.H., Reager, J.T., Famiglietti, J.S., Voss, K., Swenson, S., Rodell, M., 2015. Quantifying renewable groundwater stress with GRACE. Water Resour. Res. 51, 5217–5238.
Rodell, M., Houser, P.R., Jambor, U., Gottschalck, J., Mitchell, K., Meng, C., Arsenault, K., Cosgrove, B., Radakovich, J., Bosilovich, M., 2004. The global land data assimilation system. Bull. Am. Meteorol. Soc. 85, 381–394.
Save, H., Bettadpur, S., Tapley, B.D., 2016. High resolution CSR GRACE RL05 mascons. J. Geophys. Res. Solid Earth 121, 7547–7569.
Scanlon, B.R., Zhang, Z., Save, H., Sun, A.Y., Schmied, H.M., Beek, L.P.H.V., Wiese, D.N., Wada, Y., Di, L., Reedy, R.C., 2018. Global models underestimate large decadal declining and rising water storage trends relative to GRACE satellite data. Proc. Natl. Acad. Sci. U. S. A. 115, E1080–E1089.
Seddon, A.W.R., Maciasfauria, M., Long, P.R., Benz, D., Willis, K.J., 2016. Sensitivity of global terrestrial ecosystems to climate variability. Nature 531, 229–232.
Soni, A., Syed, T.H., 2015. Diagnosing land water storage variations in Major Indian River basins using GRACE observations. Glob. Planet. Chang. 133, 263–271.
Sugihara, G., May, R., Ye, H., Hsieh, C.-h., Deyle, E., Fogarty, M., Munch, S., 2012. Detecting causality in complex ecosystems. Science 338 (6106), 496–500.
Sun, Q., Miao, C., AghaKouchak, A., 2016. Century-scale causal relationships between global dry/wet conditions and the state of the Pacific and Atlantic Oceans. Geophys. Res. Lett. 43 (12), 6528–6537.
Tapley, B.D., Srinivas, B., Ries, J.C., Thompson, P.F., Watkins, M.M., 2004. GRACE measurements of mass variability in the Earth system. Science 305, 503–505.
Thomas, A.C., Reager, J.T., Famiglietti, J.S., Rodell, M., 2014. A GRACE- based water storage deficit approach for hydrological drought characterization. Geophys. Res. Lett. 41, 1537–1545.
Tian, F., Fensholt, R., Verbesselt, J., Grogan, K., Horion, S., Wang, Y., 2015. Evaluating temporal consistency of long-term global NDVI datasets for trend analysis. Remote Sens. Environ. 163, 326–340.
Tucker, C.J., Pinzon, J.E., Brown, M.E., Slayback, D.A., Pak, E.W., Mahoney, R., Vermote, E.F., El Saleous, N., 2005. An extended AVHRR 8-km NDVI dataset compatible with MODIS and SPOT vegetation NDVI data. Int. J. Remote Sens. 26, 4485–4498.
Velicogna, I.A.G., Kimball, J.S., Kim, Y., 2015. Impact of changes in GRACE derived terrestrial water storage on vegetation growth in Eurasia. Environ. Res. Lett. 10, 124024.
Vicente-Serrano, S.M., Gouveia, C., Camarero, J.J., Begueria, S., Trigo, R., Lopez-Moreno, J.I., Azorin-Molina, C., Pasho, E., Lorenzo-Lacruz, J., Revuelto, J., Moran-Tejeda, E., Sanchez-Lorenzo, A., 2013. Response of vegetation to drought time-scales across global land biomes. Proc. Natl. Acad. Sci. U. S. A. 110, 52–57.
Wang, H., He, B., Zhang, Y., Huang, L., Chen, Z., Liu, J., 2018a. Response of ecosystem productivity to dry/wet conditions indicated by different drought indices. Sci. Total Environ. 612, 347–357.
Wang, J., Song, C., Reager, J.T., Yao, F., Famiglietti, J.S., Sheng, Y., MacDonald, G.M., Brun, F., Schmied, H.M., Marston, R.A., Wada, Y., 2018b. Recent global decline in endorheic basin water storages. Nat. Geosci. 11, 926–932.
Watkins, M.M., Wiese, D.N., Yuan, D.N., Boening, C., Landerer, F.W., 2015. Improved methods for observing Earth's time variable mass distribution with GRACE using spherical cap Mascons. J. Geophys. Res. Solid Earth 120, 2648–2671.
Wei, Z.W., Yoshimura, K., Wang, L.X., Miralles, D.G., Jasechko, S., Lee, X.H., 2017. Revisiting the contribution of transpiration to global terrestrial evapotranspiration.

Geophys. Res. Lett. 44, 2792–2801.
Wei, X., Li, Q., Zhang, M., Giles-Hansen, K., Liu, W., Fan, H., Wang, Y., Zhou, G., Piao, S., Liu, S., 2018. Vegetation cover - another dominant factor in determining global water resources in forested regions. Glob. Chang. Biol. 24, 786–795.
Wiese, D. (2015). GRACE Monthly Global Water Mass Grids NETCDF RELEASE 5.0. Ver. 5.0. PO. DAAC, CA, USA. *Dataset accessed [2017–06-01] at doi:*https://doi.org/10.5067/TEMSC-OCL05.
Wiese, D.N., Landerer, F.W., Watkins, M.M., 2016. Quantifying and reducing leakage errors in the JPL RL05M GRACE mascon solution. Water Resour. Res. 52, 7490–7502.
Wu, D., Zhao, X., Liang, S., Zhou, T., Huang, K., Tang, B., Zhao, W., 2015. Time-lag effects of global vegetation responses to climate change. Glob. Chang. Biol. 21, 3520–3531.
Xie, Y., Huang, S., Liu, S., Leng, G., Peng, J., Huang, Q., Li, P., 2018. GRACE-based terrestrial water storage in Northwest China: changes and causes. Remote Sens. 10, 1163.
Xu, X.Y., Yang, D.W., Yang, H.B., Lei, H.M., 2014. Attribution analysis based on the Budyko hypothesis for detecting the dominant cause of runoff decline in Haihe basin. J. Hydrol. 510, 530–540.
Yang, Y.T., Long, D., Guan, H.D., Scanlon, B.R., Simmons, C.T., Jiang, L., Xu, X., 2014. GRACE satellite observed hydrological controls on interannual and seasonal variability in surface greenness over mainland Australia. J. Geophys. Res. Biogeosci. 119, 2245–2260.
Yang, X., Yong, B., Ren, L., Zhang, Y., Long, D., 2017. Multi-scale validation of GLEAM evapotranspiration products over China via ChinaFLUX ET measurements. Int. J. Remote Sens. 38, 5688–5709.
Zeng, Z., Piao, S., Li, L.Z., Wang, T., Ciais, P., Lian, X., Yang, Y., Mao, J., Shi, X., Myneni, R.B., 2018. Impact of earth greening on the terrestrial water cycle. J. Clim. 31, 2633–2650.
Zhou, L., Tian, Y., Myneni, R.B., Philippe, C., Sassan, S., Liu, Y.Y., Shilong, P., Haishan, C., Vermote, E.F., Conghe, S., 2014. Widespread decline of Congo rainforest greenness in the past decade. Nature 509, 86–90.